# Supporting Information

# Facile synthesis of $L1_0$-PtFe/C Intermetallic Catalysts with Superior Catalytic Durability for Oxygen Reduction Reaction

*Shengwei Yu, Liyuan Bi, Xiang Xie, Jiyuan Lu, Aiping Chen and Haibo Jiang\**

Shanghai Engineering Research Center of Hierarchical Nanomaterials, Key Laboratory for

Ultrafine Materials of Ministry of Education, School of Materials Science and Engineering, East

China University of Science & Technology; Shanghai 200237, China

**Experimental Section**

**1. Materials and Chemicals**

Chloroplatinic acid hexahydrate ($H_2PtCl_6 \cdot 6H_2O$, 37.5 wt%) was purchased from Adamas-beta. Ferric chloride hexahydrate ($FeCl_3 \cdot 6H_2O$, 99 wt%) was purchased from General-reagent. Urea ($CO(NH_2)_2$, 99.5 wt%) was purchased from Aladdin (Shanghai, China). Cabot Vulcan XC-72 was obtained from Macklin Biochemical Co. Ltd. (Shanghai, China). Nafion (5 wt% in lower) was ordered from Sigma-Aldrich (Milwaukee, USA). Ethanol and isopropanol were analytical reagent (A.R.) grade and purchased from Titan Scientific Co. Ltd. (Shanghai, China). Commercial Pt/C (Pt loading: 20 wt%, Pt on carbon black) was purchased from HeSen electric Co. Ltd.. All reagents were used without any further purification.

**2. Synthesis of d-PtFe/C and o-PtFe/C**

In a typical procedure to prepare d-PtFe/C, 40 mg of urea, 30 mg of carbon black (Vulcan XC-72), 1.68 mL of $H_2PtCl_6$ aqueous solution (10 mg/mL) and 11.1 mg $FeCl_3 \cdot 6H_2O$ were dispersed homogeneously by ultrasonication in ultrapure water. The aqueous solution was then freeze-dried to obtain the black powder. Subsequently, the pre-calcined black powder was placed in a tube furnace and heated to 550 °C at a rate of 10 °C/min under $H_2/Ar$ atmosphere, held for 2 h. After natural cooling, d-PtFe/C was obtained. Adjusting the ratio of $H_2PtCl_6$ aqueous solution to acquire $FeCl_3 \cdot 6H_2O$, d-$Pt_4Fe/C$, $Pt_3Fe/C$, $Pt_2Fe/C$, $Pt_{1.5}Fe/C$, PtFe/C, $PtFe_{1.5}/C$.

The preparation of o-PtFe/C was similar to that of d-PtFe/C, with the difference that heated to 550 °C at a rate of 10 °C/min and held for 2 h, subsequently, the temperature was raised to 800 °C again to induce the ordering transition of the atoms, and then the o-PtFe/C catalyst was obtained after natural cooling.

## 3. Characterization

The morphology and surface structure of the as-synthesized samples were characterized by transmission electron microscopy (TEM, JEOL-2100 transmission electron microscope with LaB6-cathode (200 kV)). Aberration-corrected high-angle annular dark-field (HAADF) scanning transmission electron microscopy (STEM) and energy-dispersive X-ray spectroscopy (EDX) were conducted on Grand ARM 300F. Inductively coupled plasma-atomic emission spectroscopy (ICP-AES, Agilent 725ES) was used to determine the composition of nanostructures. The X-ray diffraction (XRD) patterns were performed on a D8 ADVANCE (Bruker, Germany) diffractometer with Cu Kα radiation. X-ray photoelectron spectra (XPS) were collected using a Thermo Scientific ESCALAB 250 XI X-ray photoelectron spectrometer to obtain information about composition of surface elements and electronic structures.

## 4. Electrochemical Measurements

Electrochemical measurements were carried out in a three-electrode cell connected to a DH7003 electrochemical workstation. A platinum wire and saturated calomel electrode (SCE) were adopted as the counter and reference electrodes,

respectively. All the potentials were measured versus the reversible hydrogen electrode (RHE).

Before we prepared the working electrode, Catalyst inks were made by sonicating the mixture of catalyst (5 mg), isopropanol (960 µL), and Nafion (5 wt %, 40 µL) for 30 min. Appropriate amount of the ink was spread onto the glassy carbon electrode (GCE, 0.196 cm$^2$) and dried naturally for further electrochemical tests.

Cyclic voltammetry (CV) curves were obtained between 0 V and 1.3 V, in Ar-saturated 0.1 M HClO$_4$ solution at a scanning rate of 100 mV s$^{-1}$, and linear sweep voltammetry (LSV) curves were collected in O$_2$-saturated 0.1 M HClO$_4$ solution at 1600 rpm with a scanning rate of 10 mV s$^{-1}$.

The ORR kinetic current of the catalyst was obtained by the Koutecky-Levich equation:

$$i_k = \frac{i - i_l}{i i_l}$$

(1)

Where i$_k$ is the kinetic current density, i is the measured current density, and i$_l$ is the limiting current density. We took the logarithm of the kinetic current density as the abscissa and the electrode potential as the ordinate to plot the Tafel curve of the reaction, where the slope of the fitted straight line was the Tafel slope.

Accelerated durability testing (ADT) was accomplished in an O$_2$-saturated 0.1 M HClO$_4$ solution, with a potential scanning range of 0.6 ~ 1.1 V versus the reversible

hydrogen electrode at the scanning rate of 100 mV/s. The performance test was conducted every 10 k cycles.

The $CH_3OH$, HCOOH and CO resistance test were carried in the electrolyte containing 0.2 M $CH_3OH$, HCOOH and saturated CO, respectively, with a potential scanning range of 0 ~ 1.3 V versus the reversible hydrogen electrode at the scanning rate of 100 mV/s.

## 5. DFT Models and Calculations

All DFT calculations were done in the Dmol3 code. The calculation of electronic structure and exchange-correlation effects was based on the generalized gradient approximation and Perdew-Burke-Ernzerhof (GGA-PBE) functional. Valence electrons were expanded by the polarization (DNP) function of the dual value basis. The inner electrons were frozen by the semi-nuclear pseudopotential. The DFT semi-nuclear pseudopotential was used to simulate the relativistic effect. The model was built based on the structural characterization using four-layer periodic unit cells to simulate, the two layers of atoms at the bottom of the model were fixed with other atoms completely relaxed, and constructed exposed Pt (100) surfaces to simulate $L1_0$ PtFe intermetallic with a monolayer Pt skin, and the vacuum layer was set to 10 Å. d-PtFe was simulated by the model with disordered arrangement of Pt and Fe atoms.

The adsorption energies of O ($E_{ads}(O)$) were calculated via following equation: $E_{ads}(O) = E_{total} - E_O - E_*$, where $E_{total}$, $E_O$ and $E_*$ represented the total energy of adsorption system, the energy of O atom and the energy of adsorption system.

The alloy vacancy formation energy is calculated by following equation: $\Delta E_{PtFe} = [E_{PtFe} - n \cdot E_{Pt} - m \cdot E_{Fe}] / (n+m)$, where $E_{PtFe}$, $E_{Pt}$ and $E_{Fe}$ represented the energy of the constructed PtFe model, Pt atoms and Fe atoms, respectively, and n and m represented the number Pt and Fe atoms in the PtFe model.
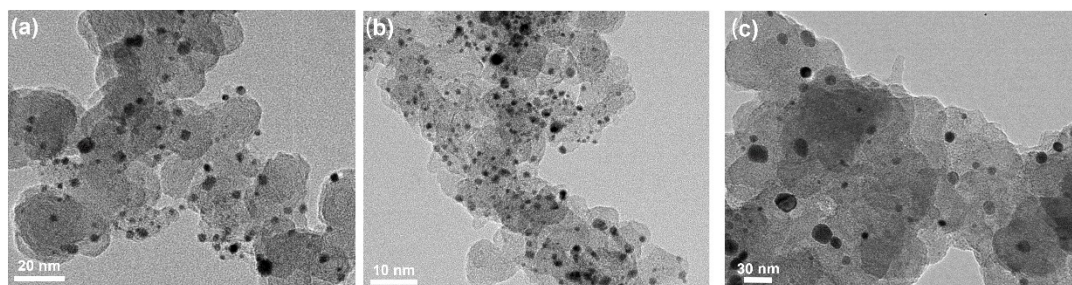
**Fig. S1 Morphology characterization of (a)** o-PtFe/C in the presence of urea, **(b)** d-PtFe/C in the presence of urea and **(c)** PtFe/C without urea addition.
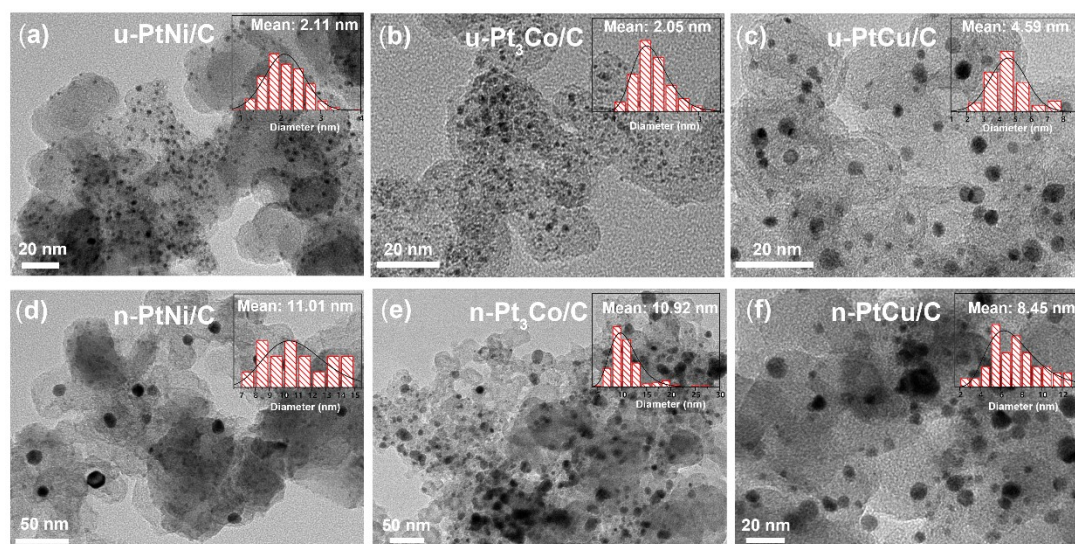


**Fig. S2 Morphology characterization of (a)** PtNi/C, **(b)** $Pt_3Co/C$, **(c)** PtCu/C in the presence of urea marked with "u-" and **(d)** PtNi/C, **(e)** $Pt_3Co/C$, **(f)** PtCu/C in the absence of urea marked with "n-".
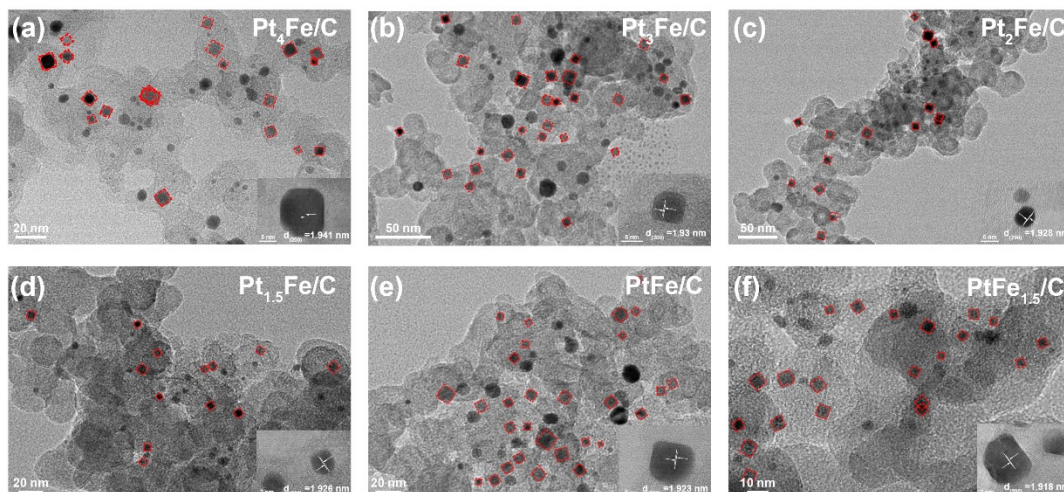
**Fig. S3 Morphology characterization of d-PtFe/C with different Pt/Fe atomic ratios.**
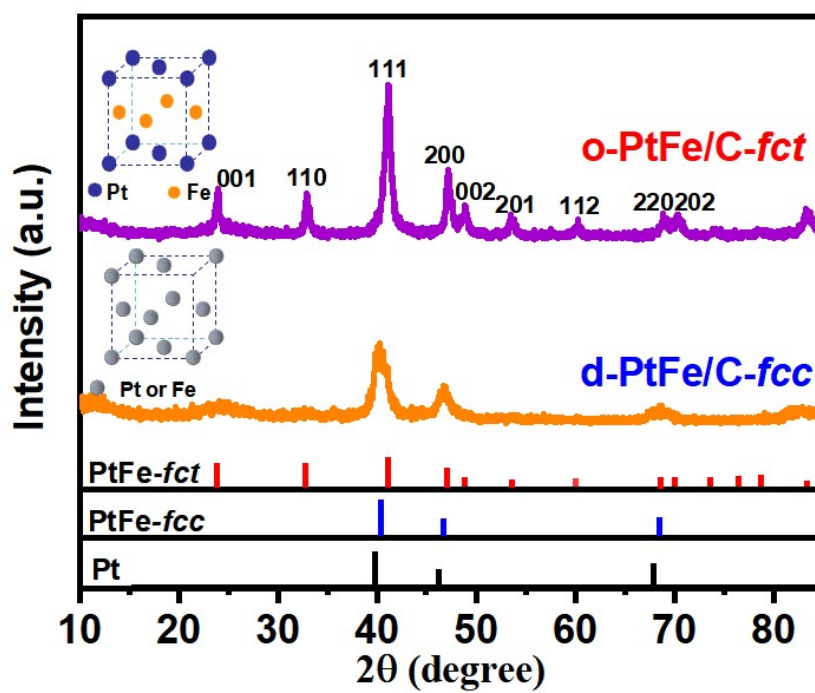


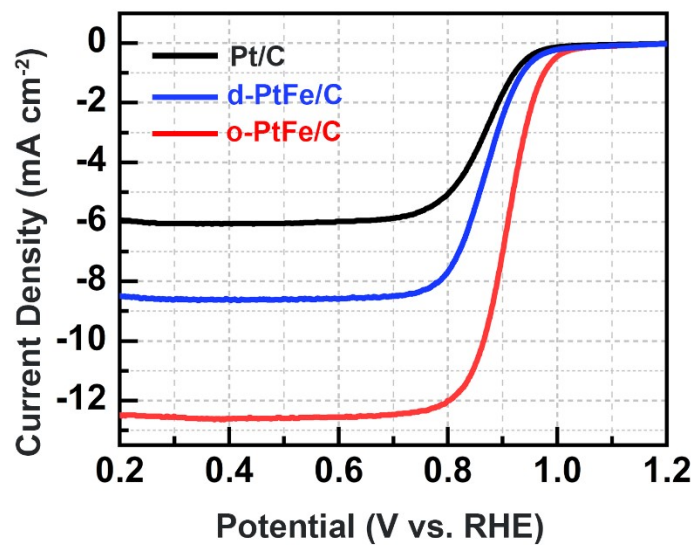**Fig. S4 X-ray diffraction patterns of o-PtFe/C and d-PtFe/C.**

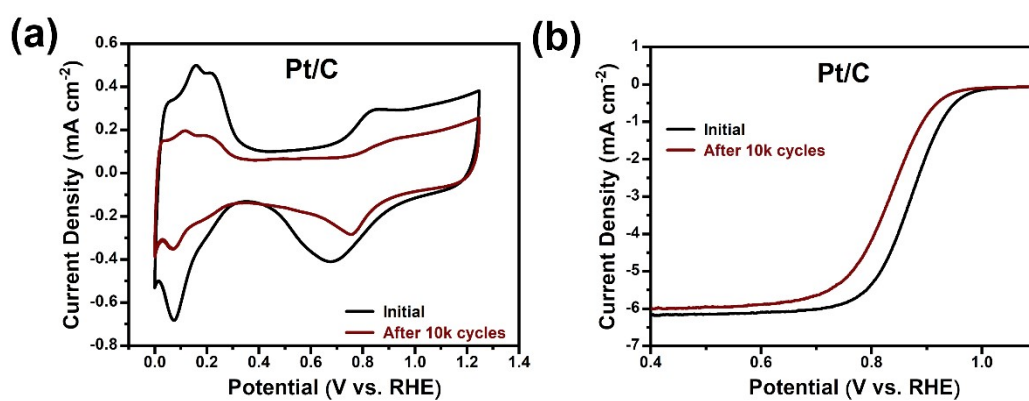**Fig. S5** LSV curves of Pt/C, d-PtFe/C and o-PtFe/C with the current density normalized to the ECSA.



**Fig. S6 CV and LSV curves of Pt/C before and after ADTs.**
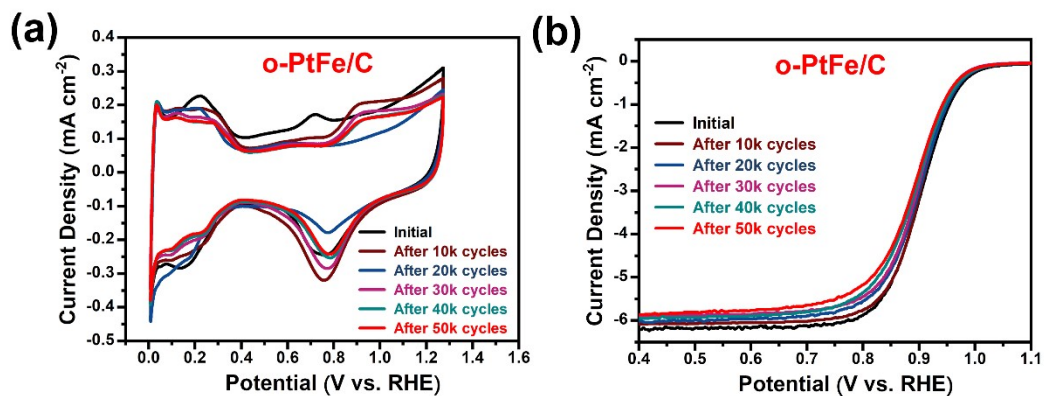
**Fig. S7 CV and LSV curves of o-PtFe/C before and after ADTs.**
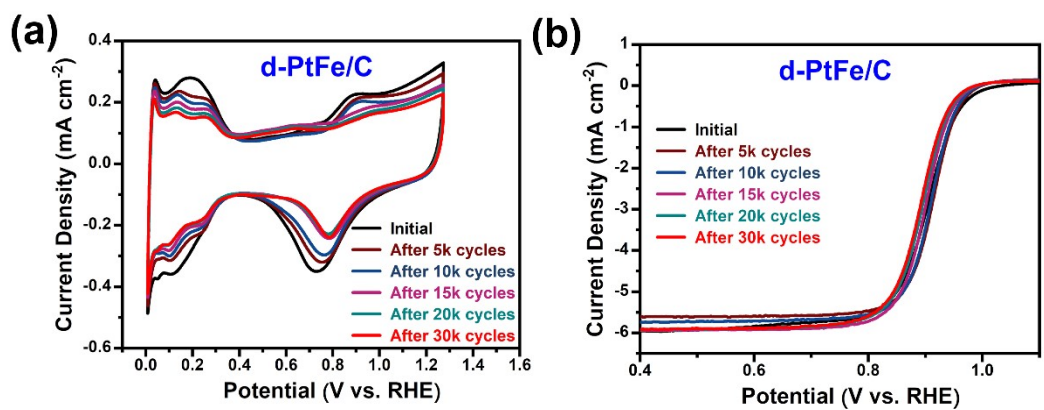
.



**Fig. S8 CV and LSV curves of d-PtFe/C before and after ADTs.**
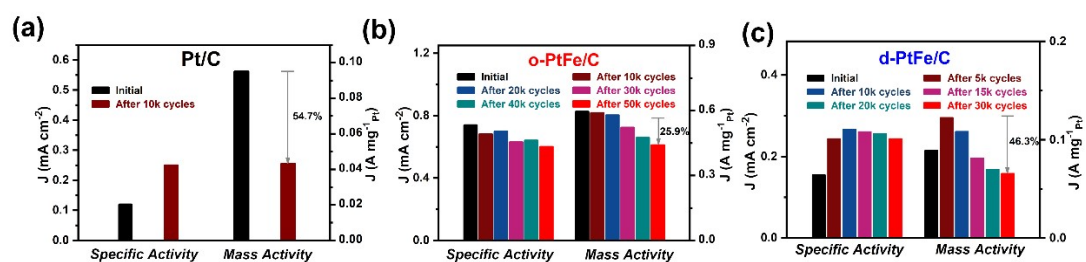


**Fig. S9 Variations in SA and MA of Pt/C, o-PtFe/C and d-PtFe/C before and after ADTs.**
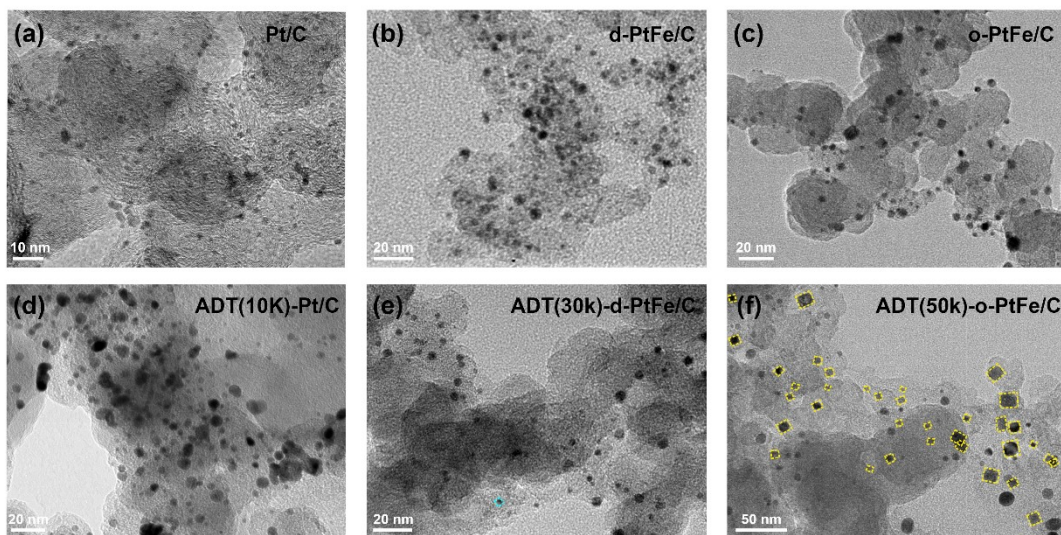
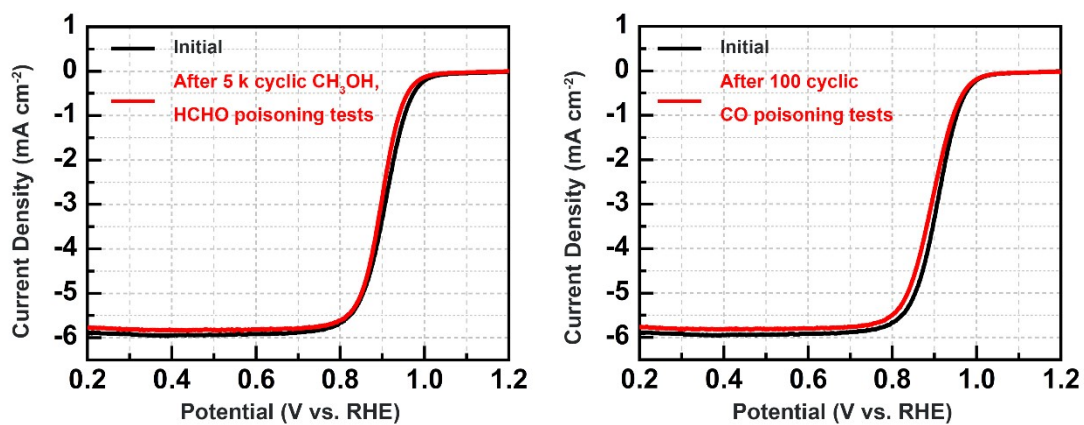**Fig. S10 Variations in Morphological of Pt/C, o-PtFe/C and d-PtFe/C before and after ADTs.**



**Fig. S11 Comparison of LSV curves between (a)** initial o-PtFe/C and that after 5000 cyclic CH₃OH and HCHO poisoning tests **(b)** initial o-PtFe/C and that after 100 cyclic CO poisoning tests.

**Table S1 Comparison among various intermetallic.**

| Intermetallic | Synthesis method | Particle size | Shape | References |
|---|---|---|---|---|
| o-PtFe/C | One-step thermal reduction | 6.6 nm | Tetragon | This work |
| Pd−Se NPs/C | Liquid-phase synthesis | 60 nm | Nanosphere | 1 |
| FePt@PtBi | Liquid-phase synthesis, heat treatment and $BiCl_3$ treatment | 4.2 nm | Nanosphere | 2 |
| subsize $Pt_3Co$ | Liquid-phase synthesis, and heat treatment | 2.3 nm | Nanosphere | 3 |
| Pt-Pd | Liquid-phase synthesis | 16.6 nm | Concave nanocube | 4 |
| PtCuNi-W/C | Liquid-phase synthesis, and acid treatment | 10 nm | Octahedron | 5 |
| PtFe | In-situ synthesis and impregnation | 3.7 nm | Nanosphere | 6 |
| PtFe | In-situ synthesis, template method and thermal treatment | 4 nm | Nanocube | 7 |
| $L1_0$-FePt | Acid etching and thermal treatment | 8 nm | Nanosphere | 8 |

**Table S2 The order degree of d-PtFe/C and o-PtFe/C calculated by XRD.**

| Samples | (001)/(111) | (001) Order degree | (110)/(111) | (110) Order degree |
|---|---|---|---|---|
| Standard PDF | 0.3 | 1 | 0.28 | 1 |
| d-PtFe/C | 0.13 | 0.43 | 0.14 | 0.5 |
| o-PtFe/C | 0.29 | 0.97 | 0.278 | 0.99 |

**Table S3 Rietveld full spectrum refinement results of d-PtFe/C and o-PtFe/C.**

|  | lattice constant | lattice volume | $R_{wp}$ (%) | $R_p$ (%) | $\chi^2$ | Space group |
|---|---|---|---|---|---|---|
| d-PtFe/C | 3.92 | 60.41 | 8.94 | 4.32 | 1.11 | P4/mmm (123) |
| o-PtFe/C | 3.85 | 55.35 | 9.85 | 5.14 | 1.12 | Fm-3m (225) |

**Table S4 Atomic position information in Rietveld full spectrum refinement results of d-PtFe/C and o-PtFe/C.**

|  |  | Atomic position | | | Temperature factor |
|---|---|---|---|---|---|
|  |  | x | y | z |  |
| d-PtFe/C | Pt | 0 | 0 | 0 | 0.844 |
|  | Fe | 0 | 1/2 | 1/2 | 2.244 |
| o-PtFe/C | Pt | 0 | 0 | 0 | 3.001 |

**Table S5 Deconvolution parameters of the Pt 4f for Pt/C, d-PtFe/C and o-PtFe/C.**

|  |  | Pt/C | d-PtFe/C | o-PtFe/C |
|---|---|---|---|---|
| $Pt^0/Pt^{2+}$ |  | 0.97 | 1.32 | 2.82 |
| Peak Position (eV) | Pt $4f_{7/2}$ | 71.82 | 71.72 | 71.69 |
|  | Pt $4f_{5/2}$ | 75.32 | 75.05 | 75.2 |

**Table S6 Stability comparison among various intermetallic.**

| Intermetallic | MA loss after ADTs | 10 k | 20 k | 30 k | 50 k | References |
|---|---|---|---|---|---|---|
| o-PtFe/C | | 1.0% | 2.7% | 12.3% | 25.9% | This work |
| Pt/C | | 54.7% | — | — | — | This work |
| Pd−Se NPs/C | | 21.0% | 28.2% (15 k) | — | — | 1 |
| FePt@PtBi | | 11.0% | — | 18.0% | — | 2 |
| subsize $Pt_3Co$ | | 8.0% | — | 18.5% | — | 3 |
| Pt-Pd | | — | 25.6% (15 k) | — | — | 4 |
| PtCuNi-W/C | | — | 34.1% | — | — | 5 |
| PtFe | | — | — | 29% | — | 6 |
| PtFe | | 17.0% | 21.0% | 22.0% | — | 7 |
| $L1_0$-FePt | | 3.9% | — | — | — | 8 |

**References**

1. Z. Yu, S. Xu, Y. Feng, C. Yang, Q. Yao, Q. Shao, Y. F. Li and X. Huang, *Nano Lett*, 2021, **21**, 3805-3812.

2. J. Guan, S. Yang, T. Liu, Y. Yu, J. Niu, Z. Zhang and F. Wang, *Angew Chem Int Ed Engl*, 2021, **60**, 21899-21904.

3. H. Cheng, R. Gui, H. Yu, C. Wang, S. Liu, H. Liu, T. Zhou, N. Zhang, X. Zheng, W. Chu, Y. Lin, H. Wu, C. Wu and Y. Xie, *Proc Natl Acad Sci U S A*, 2021, **118**.

4. R. Wu, P. Tsiakaras and P. K. Shen, *Applied Catalysis B: Environmental*, 2019, DOI: 10.1016/j.apcatb.2019.03.045.

5. W. Tu, K. Chen, L. Zhu, H. Zai, B. E, X. Ke, C. Chen, M. Sui, Q. Chen and Y. Li, *Advanced Functional Materials*, 2019, DOI: 10.1002/adfm.201807070.

6. Y. He, Y. L. Wu, X. X. Zhu and J. N. Wang, *ACS Appl Mater Interfaces*, 2019, DOI: 10.1021/acsami.9b01810.

7.    C. L. Yang, L. N. Wang, P. Yin, J. Liu, M. X. Chen, Q. Q. Yan, Z. S. Wang, S. L. Xu, S. Q. Chu, C. Cui, H. Ju, J. Zhu, Y. Lin, J. Shui and H. W. Liang, *Science*, 2021, **374**, 459-464.

8.    J. Li, Z. Xi, Y. T. Pan, J. S. Spendelow, P. N. Duchesne, D. Su, Q. Li, C. Yu, Z. Yin, B. Shen, Y. S. Kim, P. Zhang and S. Sun, *J Am Chem Soc*, 2018, **140**, 2926-2932.